Effect of heat treatment on the structure and magnetic properties of Sm-Fe alloys obtained by mechanical alloying

Nikolay G. Razumov[*], Aleksandr S. Verevkin, Anatoly A. Popovich

Peter the Great Saint-Petersburg Polytechnic University, St. Petersburg, 195251, Russia

[*]Corresponding author. Tel: +7 (812) 5526623; E-mail: n.razumov@onti.spbstu.ru

Abstract

The effect of heat treatment on the structure and magnetic properties of Sm-Fe alloys obtained by mechanical alloying was investigated. The crystallization temperature of Sm_2Fe_{17}, an amorphous alloy obtained by mechanical alloying, was determined using differential scanning calorimetry. Based on these results, various samples were annealed at different isothermal holding temperatures, and those with the best magnetic properties were found. Experimental studies show that decreasing the isothermal holding temperature from 750 °C to 630 °C increases magnetic characteristics nearly four times. The saturation magnetization, romance and coercivity of the Sm_2Fe_{17} powder were 121 emu/g, 28.5 emu/g and 800 Oe, respectively. Copyright © 2017 VBRI Press.

Keywords: Mechanical alloying, magnetic materials, Sm_2Fe_{17}, magnetic properties.

Introduction

Many researchers have become interested in the nitrides and carbides of the intermetallic compound Sm_2Fe_{17} because of their excellent magnetic properties, discovered by Coey and Sun in 1990 [1]. This intermetallic material is a promising replacement for permanent magnets that is different from widely-used Nd-based magnets. It has uniaxial anisotropy with a high anisotropic field and a Curie temperature exceeding 450 °C.

Several techniques have been developed for syntheszing Sm_2Fe_{17}-type magnetic materials, including casting [2], melt spinning, hydrogen disproportionation desorption recombination [3], reduction–diffusion [4], and mechanical alloying (MA) [5]. In all cases, MA proved to be an efficient technique for the low cost, large scale production of powders [2, 6]. Mechanical alloying has been recognized as a technique for synthesizing ultrafine powder materials through solid-state diffusion under intense mechanical deformations [7, 8], and MA elevates coercivity [9].

Numerous published reports have established that the master alloy, Sm_2Fe_{17}, produced via MA, consists of two main parts: nanosized crystalline α-Fe and an amorphous Sm-Fe phase [10, 11]. Heat treatment of the as-milled powder in a vacuum is required to obtain fully crystalline Sm_2Fe_{17}. The grain size can be modified by heat treating. Generally, the Sm-Fe alloy is isothermallly held between 700 °C and 850 °C; greater temperatures have been used [5, 8, 12, 13]. A single-phase Sm_2Fe_{17} intermetallic compound with a rhombohedral Th_2Zn_{17} crystal structure forms during heat treatment. A strong relationship between particle and grain size and magnetic properties exists.

In this paper, we describe studies of the effect of heat treatment on the structure and magnetic properties of non-nitrogenated Sm-Fe alloys obtained by MA. The crystallization temperature of partially amorphous Sm-Fe alloys was determined using differential scanning calorimetry (DSC). The results led us to anneal various samples at different isothermal holding temperatures and compare their magnetic properties. Grain size, lattice parameters, and magnetic properties were functions of the isothermal holding temperature.

Experimental

Materials

High purity Fe (d90 < 300 μm, 99.96% purity; NevaReaktiv, LLC, Russia) and Sm (d90 < 700 μm, 99.9% purity; Huizhou Gl Technology Co., LTD, PRC) were used as initial components.

Preparation of Sm-Fe powders

Sm-Fe-based alloys were prepared by MA of initial powders using a Pulverisette-4 vario-planetary mill (Fritsch GmbH, Germany). This technique applies a short isothermal holding time. The obtained nanocrystalline powders are very reactive and are easily subjected to nitriding. Moreover, nanocrystalline materials have an adapted microstructure for extrinsic magnetic properties [14].

To prevent oxidation of the initially-formed powder, all operations were handled inside a glove box under a high-purity nitrogen atmosphere. Powders initially nominally composed of Fe and 15 at.% Sm (5 at.% excess Sm) were milled for 10 h using a planetary ball mill with hard metal vials and balls under an argon atmosphere and a ball-to-powder mass ratio of 10:1 using a disc rotation velocity of 200 rpm. The main-to-planetary disc rotation velocity ratio was 1:-1.5. The as-milled powders were annealed in a vacuum furnace (VBF-1200X; MTI Corporation, USA) under a medium vacuum of about 150 mtorr at 630 °C to 750 °C for 30 minutes. The excess 5 at.% Sm was used to compensate for possible Sm evaporation during the isothermal hold.

Characterizations

The powder morphology and distribution of elements per volume of powder particle were examined using a scanning electron microscope (Mira 3 Tescan; Tescan Orsay Holding a.s, Czech Republic) at 20 kV equipped with an Oxford INCA Wave 500 add-on device.

Thermal analysis was performed using a DSC device for thermal testing of materials (Setaram SETSYS Evolution 16; Setaram Instrumentation SAS, France) under an argon flow of 30 ml min-1, a heating rate of 5 °C min-1, and a temperature range of 20 °C to 1000 °C.

The crystal structures of the obtained powders were characterized by X-ray diffraction (XRD) on a Brucker D2 Phaser (Bruker Corporation, USA) in Co-Kα-radiation (λ = 1.79026 Å) at a scanning step of 0.05° (2θ scale) for 0.5 s in the range of 2θ = 30° to 100°. TOPAS software was used to carry out the Rietveld refinement of the XRD patterns and to analyze the crystal structures and calculate the lattice parameters and grain size. The quality of the Rietveld refinement was evaluated in terms of goodness of fit (GOF) and the R factor (R_{wp}). Generally, when GOF is close to 1 and R_{wp} is less than 10%, the result can be considered reliable.

Magnetic properties were measured at ambient temperature (300 K) using a vibrating sample magnetometer (Lakeshore 7410 model VSM; Lake Shore Cryotronics, Inc, USA) at the maximum magnetic field of 22 kOe, a measurement sensitivity of 4 emu, and a measurement step of 200 Oe.

Results and discussion

Powder morphology

The SEM micrographs in **Fig. 1a** and **1b** show the morphologies of as-milled Sm_2Fe_{17} powders. The as-milled powder appeared in the form of irregular highly agglomerated particles with an average size of 8 µm. The elemental analysis obtained by energy-dispersive X-ray spectroscopy indicated uniform and homogeneous distribution of each initial element in the particle. The XRD results showed that a two-phase mixture of amorphous Sm-Fe and α-Fe was formed in the powder. The broadening peaks corresponded to α-Fe (110) and (200) planes and showed grain refinement and an accumulation of defects and strains induced by MA.
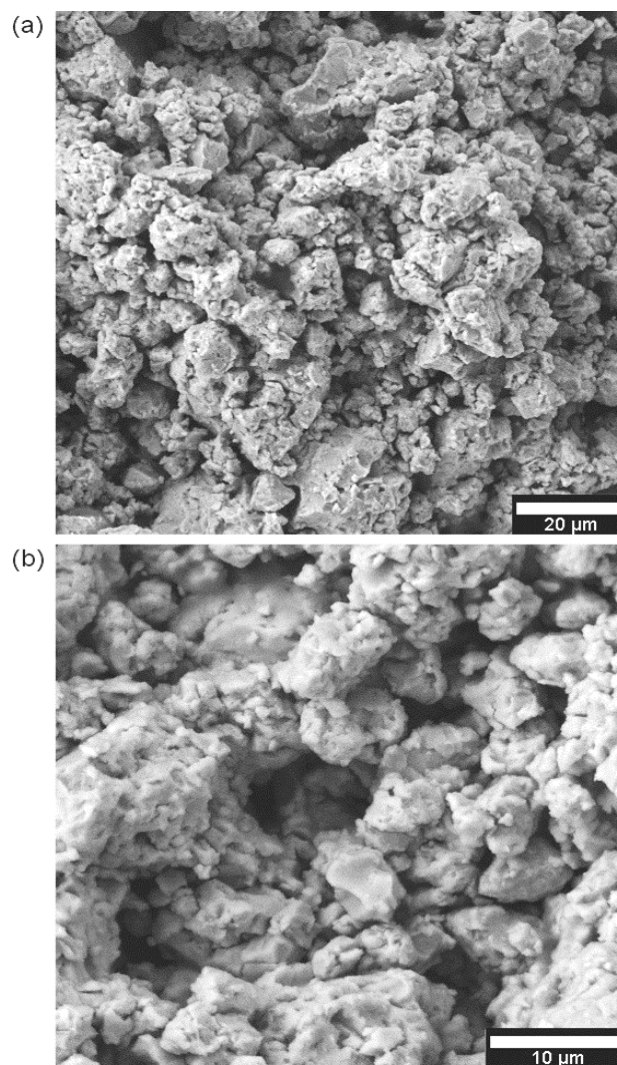

Fig. 1. SEM micrographs of as-milled powder.

DSC Measurements

The crystallization temperature of the amorphous Sm_2Fe_{17} alloy was determined using DSC, yielding three characteristic peaks as shown in **Fig. 2**.
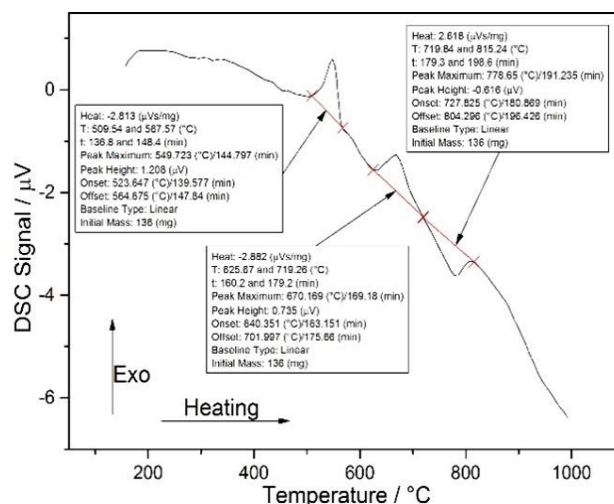

Fig. 2. Differential scanning calorimetry curve of the Sm_2Fe_{17} alloy obtained by mechanical alloying.

The first peak corresponded to the formation $SmFe_3$ phases. Tan [13] showed that the free energy barrier for the nucleation of $SmFe_3$ is smaller than that of Sm_2Fe_{17}, thus the reaction $Sm + 3Fe \rightarrow SmFe_3$ proceeds at lower temperatures. Small thermal fluctuations at 510 °C to 570 °C cannot agitate nucleations in Sm_2Fe_{17} at appreciable rates. The second peak corresponded to the formation Sm_2Fe_{17} phases. This stable chemical compound was found to form at 626 °C to 719 °C, and this was confirmed by XRD. The third peak was not determined, but the XRD phase compositions did not change with increasing heat treatment temperature. Therefore, this peak likely corresponds to the formation $SmFe_2$ phases, though this was not indicated by XRD analysis. As shown in [13], the free energy barrier for nucleation of $SmFe_3$, $\Delta G(SmFe_3)$, is lower than those for $SmFe_2$ or Sm_2Fe_{17}. $\Delta G(SmFe_3)$ being less than $\Delta G(Sm_2Fe_{17})$ can be associated with the elimination of a larger number of Sm/Fe interfaces during nucleation of $SmFe_3$, and $\Delta G(SmFe_3)$ being less than $\Delta G(SmFe_2)$ can be associated with lower driving forces for the reaction leading to the formation of $SmFe_2$. Based on these results, a series of experiments was designed to determine the effect of heat treatment on the magnetic properties of Sm_2Fe_{17} alloy.
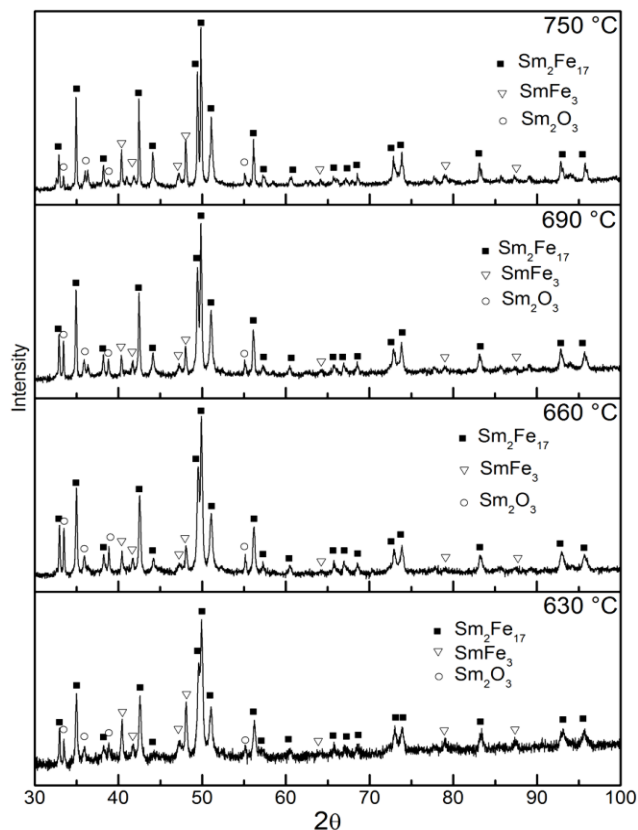

Fig. 3. X-ray diffraction patterns of Sm_2Fe_{17} alloy after isothermal hold at various temperatures.

XRD measurements

Fig. 3 shows the XRD patterns after isothermal holds at 630 °C, 660 °C, 690 °C, and 750 °C. All XRD patterns for these annealed powders were successfully indexed based on Sm_2Fe_{17}, $SmFe_3$, and Sm_2O_3. The Sm_2Fe_{17} rhombohedral Th_2Zn_{17}-type phase was shown by the main diffraction peaks (00-051-0910 pattern) at 34.92°, 42.44°, 49.42°, 49.85°, 51.09°, and 56.13°, corresponding to the (113), (300), (220), (303), (006), and (223) crystal planes. The peaks on all three XRD patterns at 40.35°, 41.85°, 47.22°, 48.03°, and 64.17° corresponded to the (110), (113), (021), (202), and (211) crystal planes of $SmFe_3$ (00-050-1450 pattern). The diffraction peaks at 33.45°, 35.95°, 38.85°, and 55.15° corresponded to the (222), (321), (400), and (440) crystal planes of Sm_2O_3 (00-015-0813 pattern). The $SmFe_3$ was formed because the Sm content in the initial powder mixture was higher than that required for formation of a nominal Sm_2Fe_{17} phase. This excess was included to account for possible losses of Sm during heat treatment or additions of α-Fe from wear debris from the vials and balls during MA. Peaks for the free α-Fe phase were not detected. Decreasing the isothermal holding temperature from 750 °C to 630 °C led to a simultaneous broadening and shifting of the Sm_2Fe_{17} diffraction peaks.
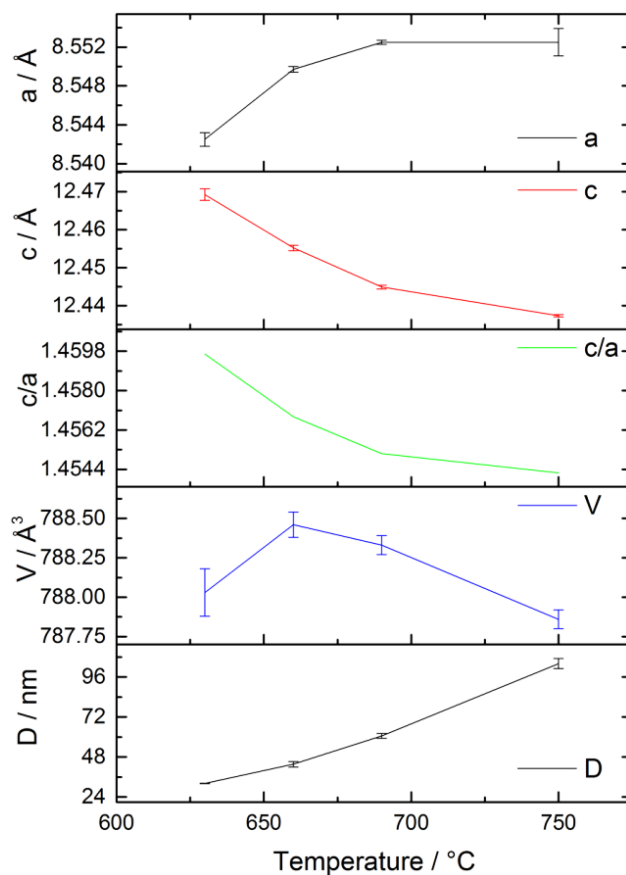

Fig. 4. Lattice parameters a and c, c/a ratio, unit-cell volume (V), and grain size (D) of Sm_2Fe_{17} alloy as a function of heat treatment temperature.

The best Rietveld refinement (GOF = 1.23; R_{wp} = 3.34%) was for powder annealed at 630 °C, resulting in three crystalline phases. One was Sm_2Fe_{17} with lattice parameters a = 8.5425(7) Å, c = 12.4692(15) Å, and V = 788.03(15) Å^3. Another was $SmFe_3$ with lattice parameters a = 5.1837(5) Å, c = 24.856(7) Å, and V = 578.4(2) Å^3. The third was Sm_2O_3 with lattice parameters a = 10.9350(15) Å and V = 1307.6(5) Å^3. Increasing the

isothermal holding temperature to 750 °C changed the lattice parameters from a = 8.5425(2) to a = 8.55253(14) Å and from c = 12.4692(2) to c = 12.4374(3)Å. The largest lattice volume was achieved at 660 °C and was 788.46(8) Å^3. The relative changes in the lattice parameters a, c, and V can be seen in **Fig. 4**. The corresponding Rietveld refinement GOF and R$_{wp}$ values were 1.47 and 2.55% when the hold temperature was 660 °C, 1.44 and 2.61% when it was 690 °C, and 1.41 and 2.57% when it was 750 °C. The Rietveld refinement results of the Sm$_2$Fe$_{17}$ alloy XRD patterns are shown in **Table 1**.

Table 1. Crystallographic parameters from the Rietveld refinement of Sm$_2$Fe$_{17}$ alloys annealed at various temperatures.

Heat treatment temperature, °C	Lattice parameters			D (nm)
	a (Å)	**c (Å)**	**V (Å^3)**	
630 °C	8.5425(7)	12.4692(15)	788.03(15)	32.2(2)
660 °C	8.5497(3)	12.4552(7)	788.46(8)	43.7(16)
690 °C	8.5525(2)	12.4449(5)	788.33(6)	60.7(15)
750 °C	8.5525(14)	12.4374(3)	787.86(1)	104(3)

Notes: V = unit cell volume; D = grain size.

The c parameter of the Th$_2$Zn$_{17}$-unit cell decreased, and the a parameter increased, with greater isothermal holding temperatures (**Fig. 4**). The c/a ratio showed that the c parameter grew at a higher rate than the a parameter decreased. This preferential distortion of the Th$_2$Zn$_{17}$-unit cell along the a- and c-axes may be indicative of remaining defects and strains after low-temperature isothermal holding. The diffraction peaks of the Sm$_2$Fe$_{17}$, SmFe$_3$, and Sm$_2$O$_3$ phases narrowed with rising isothermal holding temperature, indicating better crystallinity at higher temperatures. The volume of the Th$_2$Zn$_{17}$ phase was extracted by Rietveld refinement of the XRD data. The overall volume of the unit cell increased with increasing temperature, up to 660 °C. Thereafter, it decreased with temperature (**Fig. 4**).

The XRD data also showed that, as a result of isothermal holding at 630 °C, a nanocrystalline structure was formed with a grain size of 32(2) nm. Crystal size increased with isothermal holding temperature to 100 to 110 nm.

Magnetic measurements

Hysteresis loops for non-magnetized samples are presented in **Fig. 5**. It can be seen that the coercive force of the samples increased from 200 to 800 Oe through increases in isothermal holding temperature (**Fig. 5a**). Coercivity increased with grains size reduction (**Table 1**). Yosida **[15]** and Khazzan *et al.* **[16]** showed that the coercive field value and the magnetization reversal process depend not only on chemical composition, temperature, and magnetic anisotropy, but also strongly on microstructure. Higher coercivities can be achieved when grains are finer **[15, 18]**. When isothermal holding temperature is low, the sample often has many defects resulting from high-energy milling; in this case, crystallite sizes are very small. It is well known that crystalline size increases with isothermal holding temperature. Therefore,

grain size is optimal after an isothermal hold at 630 °C. The c parameter and grain size were found to be strongly correlated to magnetic properties.
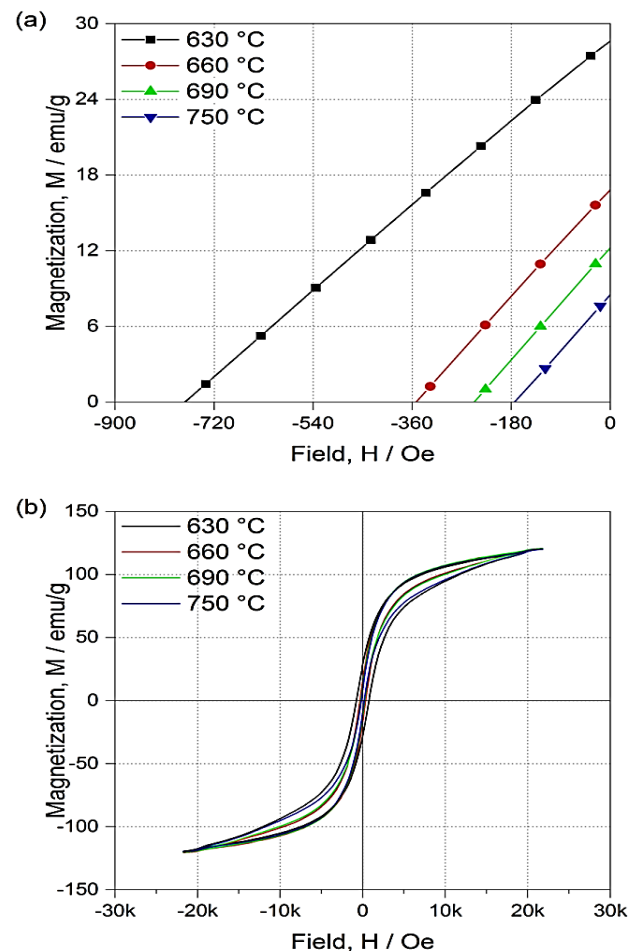

Fig. 5. Hysteresis loops of Sm$_2$Fe$_{17}$ alloys formed using isothermal holds at various temperatures.

As depicted in **Table 2**, most Sm$_2$Fe$_{17}$ powders, produced using different processes that resulted in much larger grain or particle sizes, (0.3 to 20 μm), showed much lower coercivities, ranging between 240 and 480 Oe. This is the result of the size effect of the Sm$_2$Fe$_{17}$ powder. Only Yun *et al.* **[19]** used a modified reduction-diffusion process to synthesize Sm$_2$Fe$_{17}$ nanopowders, achieving coercivities greater than 1000 Oe.

Table 2. Magnetic properties of Sm$_2$Fe$_{17}$ alloy synthesized by various processes.

Process	Particle size, D (μm)	Coercivity, H$_c$ (Oe)	Saturation Magnetization, M$_s$ (emu/g)	Ref.
MA	8	800	121	This study
MRD process	0.1-0.3	1000	128	**[19]**
Arc melting	<50	300	110	**[23]**
Induction melting	<25	550	117	**[24]**
R-D process	5-10	300	110-130	**[4]**
HDDR	<3	600	130	**[3]**

Conclusion

Formation temperature range of the stable chemical compound Sm_2Fe_{17} was determined using DSC. Best magnetic properties archived 630 °C. This temperature corresponds to the beginning of the Sm_2Fe_{17} formation. In Sm_2Fe_{17}, the single domain is approximately 350 nm [**20**]. Below this grain size, coercivity should rapidly reduce with grain size; we observed abnormal coercivity in ultrafine crystallite powders. The field of 22 kOe wich may be generated by VSM magnetometer are below magnetization field required for saturation of approx. 40 kOe [**21**] of Sm_2Fe_{17} intermetallic compound. Proper magnetization might result in better magnetic values [**22**].
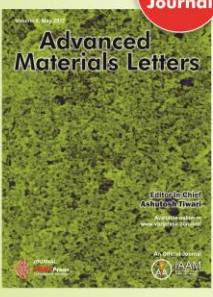
Author's contributions

Conception of the plan: Nikolay G. Razumov, Anatoly A. Popovich. Experimental work: Aleksandr S. Verevkin. Data analysis: Nikolay G. Razumov, Aleksandr S. Verevkin. Manuscript preparation: Nikolay G. Razumov, Aleksandr S. Verevkin. Manuscript review: Anatoly A. Popovich. All authors are free of competing financial interests.

References

1. Coey, J.M.D.; Sun, H. *J. Magn. Magn. Mater.* **1990**, *87*(3), L251.
   DOI: 10.1016/0304-8853(90)90756-G
2. Imaoka, N.; Iriyama, T.; Itoh, S. *J. Alloy Comp.* **1995**, *222*(1), 73.
   DOI: 10.1016/0925-8388(94)04920-3.
3. Sun, J.B.; Cui, C.X.; Zhang, Y.; Wang, R.; Li, L.; Yang, W.; Liu, Y.L. *Mater. Chem. Phys.* **2006**, *97*(1), 116.
   DOI: 10.1016/j.matchemphys.2005.07.058.
4. Lee, J.-G.; Kang, S.-K.; Si, P.-Z.; Choi, C.-J. *J. Magn.* **2011**, *16*(2), 104.
   DOI: 10.4283/JMAG.2011.16.2.104.
5. Popovich, A.A.; Verevkin, A.S.; Razumov, N.G.; Popovich, T.A. *ARPN J. Eng. Appl. Sci.* **2016**, *11(3)*, *1745*.
6. Fang, Q.; An, X.; Wang, F.; Li, Y.; Du, J.; Xia, W.; Yan, A.; Liu, J.P.; Zhang, J. *J. Magn. Magn. Mater.* **2016**, *410*, 116.
   DOI: 10.1016/j.jmmm.2016.03.029
7. Lee, C.H.; Fukunaga, T.; Yamada, Y.; Mizutani, U.; Okamoto, H. *J. Phase Equilib.* **1993**, *14*, 167.
   DOI: 10.1007/BF02667804
8. Lee, C.-H.; Kwon, Y.-S. *Met. Mater. Int.* **2002**, *8*(2), 151.
   DOI: 10.1007/BF03027011
9. Lv, X.; Liu, W.; Cui, W.; Zhao, X.; Ren, W.; Zhang, Z. *J. Appl. Phys.* **2008**, *103*, 07E122.
   DOI: 10.1063/1.2830021
10. Schultz, L.; Schnitzke, K.; Wecker, J.; Katter, M.; Kuhrt, C. *J. Appl. Phys.* **1991**, *70*(10), 6339.
    DOI: 10.1063/1.349962.
11. Majima, K.; Niimi, N.; Katsuyama, S.; Nagai, H.; Tomizawa, H. *J. Alloy Comp.* **1993**, *193*(1), 268.
    DOI: 10.1016/0925-8388(93)90367-V.
12. Kuhrt, C.; Schnitzke, K.; Schultz, L. *J. Appl. Phys.* **1993**, *73*(10), 6026.
    DOI: 10.1063/1.353458
13. Tan, M. *J. Mater. Sci.* **1994**, *29*(5), 1306.
    DOI: 10.1007/BF00975080
14. Nehdi, I.; Bessais, L.; Djega-Mariadassou, C.; Abdellaoui, M.; Zarrouk, H. *J. Alloy Comp.* **2003**, *351*, 24.
    DOI: 10.1016/S0925-8388(02)01033-2.
15. Yoshida, Y. Recent Developments in High Performance NdFeB Magnets and Bonded Rare-Earth Magnets. Int. Forum Magn. App. Tech. Mat., Jacksonville, Fl, USA, 21-22 January 2016 [url:http://www.magneticsmagazine.com/conferences/2016/Presentations/Daido_Yoshida_Magnetics2016.pdf]
16. Khazzan, S.; Bessais, L.; Van Tendeloo, G.; Mliki, N. *J. Magn. Magn. Mater.* **2014**, *363*, 125.
    DOI: 10.1016/j.jmmm.2014.03.030
17. Uestuener, K.; Katter, M.; Rodewald, W. *IEEE Trans. Magn.*, **2006**, *42*(10), 2897.
    DOI: 10.1109/TMAG.2006.879889.
18. Chen, C.H.; Kodat, S.; Walmer, M.H.; Cheng, S.F.; Willard, M.A.; Harris, V.G. *J. Appl. Phys.* **2003**, *93*(10), 7966.
    DOI: 10.1063/1.1558272.
19. Yun, J.-C.; Yoon, S.-M.; Lee, J.-Y.; Choi, J.-P.; Lee, J.-S. *Mater. Trans.* **2014**, *55*(10), 1630.
    DOI: 10.2320/matertrans.M2014152
20. Kobayashi, K.; Rao, X.-L.; Coey J.M.D.; Givord, D. *J. Appl. Phys.* **1996**, *80*, 6385.
    DOI: 10.1063/1.363638.
21. Isnard, O.; Miraglia, S.; Guillot, M.; Fruchart, D. *J. Appl. Phys.* **1994**, *75*(10), 5988.
    DOI: 10.1063/1.355485.
22. Przybylski, M.; Kapelski, D.; Ślusarek, B.; Wiak, S. *Sensors* **2016**, *16*(4), 569.
    DOI: 10.3390/s16040569.
23. Zhao, L.; Zheng, L. *Funct. Mat. Let.* **2013**, *6*(4), 1350038(1).
    DOI: 10.1142/S1793604713500380
24. Saito, T.; Miyoshi, H.; Nishio-Hamane, D. *J. Alloy Comp.* **2012**, *519*, 144.
    DOI: 10.1016/j.jallcom.2011.12.156